Research Article
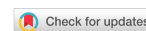
Nitrogen sulfur dual-doped porous biochar fibers for high performance lithium-sulfur battery

Xuefeng Li[1,#], Kaige Sun[2,#]

[1]Department of Chemical and Biological Engineering, Monash University, Clayton, VIC 3800, Australia.
[2]School of Chemical Engineering, The University of Queensland, St Lucia, QLD 4072, Australia.
#The authors contributed equally to this work.

Correspondence to: Dr. Xuefeng Li, Department of Chemical and Biological Engineering, Monash University, Wellington Rd, Clayton, VIC 3800, Australia. E-mail: xuefeng.li@monash.edu

Abstract

Porous carbons have gained great attention for applications in lithium-sulfur (Li-S) batteries. However, achieving high specific surface area, hierarchical porosity, and abundant heteroatom-doping with facile approaches is still challenging. Herein, nitrogen, sulfur dual-doped porous biochar fibers (PBF@N@S) are obtained *via* a simple and sustainable activation process of cotton fibers. The as-prepared PBF@N@S exhibits a hierarchically interconnected network porous structure and large specific surface area. Meanwhile, abundant nitrogen, sulfur atoms are simultaneously doped in the carbons. These characteristics make the carbon favorable for hosting sulfur. The PBF@N@S sample with 50 *wt*% sulfur content (PBF@N@S-S-50%) delivers a high initial capacity with excellent cycling performance. Such high performance suggests that the PBF@N@S-S could be a promising cathode material for Li-S batteries.

Keywords: Biomass carbon, hierarchical porous structure, N, S co-doping, Li-S batteries

INTRODUCTION

Rechargeable lithium (Li) batteries have played an extraordinary role in portable electronics[1-3]. In the 1990s, Li-ion batteries (LIBs) were successfully commercialized and dominated the energy storage market, led by Sony Company[4]. However, traditional LIBs are reaching their theoretical limits, and there are still

challenges in many aspects, such as low specific capacity and energy density, cost, and safety[5,6]. Over the past few years, multielectron reactions have drawn lots of attention as an efficient way for designing and developing high-performance batteries. Particularly, compared to traditional LIBs, Li-sulfur (Li-S) batteries have attracted lots of interest because of their remarkable specific capacity (1,675 mAh/g) and high energy density (2,500 wh/kg)[7-9]. In addition, S, as the active material of cathodes, has plenty of advantages, such as cheap, natural abundance, and eco-friendly[10,11]. Moreover, Li-S batteries offer more safety than commercialized Li-ion batteries because the highly reactive Li anode is passivated with sulfide during operation. As a result, Li-S batteries have attracted more interest and have been considered as one of the most popular candidates for energy storage.

Unfortunately, up to now, the practical application of Li-S batteries is still obstructed by three unsolved issues: (1) the insulating nature of sulfur and lithium sulfides (5×10^{-30} S/cm at 25 ℃); (2) the "shuttle effect" occurred between cathode and lithium anode causing irreversible loss of S; (3) the significant changes of structural and volume in the charge/discharge process[12,13]. To address the above issues, a number of strategies have been made. Among them, incorporating S with highly conductive carbon materials, such as porous carbon, graphene, and carbon nanotubes, is one of the most promising strategies for high-performance Li-S batteries[14-16]. The carbon framework can greatly enhance electron transport, suppress the diffusion of polysulfides, and improve the ability to withstand volume variations of the active material. In addition, doping heteroatoms into carbon materials can adjust the local bonding environment and electron distribution of the carbon surface[17,18]. For instance, the introduction of electronegative nitrogen (N) atoms into the carbon can affect the net polarity and promote the interaction of S atoms with the carbon matrix[19]. S doping can also enhance the affinity of polysulfides to the carbons[20]. Niu *et al.* prepared a N, S co-doped porous carbon sphere through hydrothermal activation methods, which delivered a high initial capacity of 942 mAh/g as a Li-S battery cathode[20]. Kim *et al.* synthesized N, S co-doped porous carbon via a hydrothermal reaction of graphene and methylene blue. As a Li-S battery cathode, it showed a good specific capacity along with good stability[21]. Díez *et al.* produced N, S co-doped carbon nanoparticles through the pre-carbonization activation method, which delivered a reversible capacity of 841 mAh/g after 100 cycles as Li-S battery cathodes[22]. However, the synthesis of porous carbon materials, especially with heteroatom doping, suffers from a complex synthesis process and expensive raw materials and lacks scalability and consistency[23-25]. Therefore, it is necessary to develop and utilize inexpensive, environmentally friendly, and facile approaches to construct high-performance porous carbon materials.

The porous biochar prepared from biomass is attracting increasing attention due to its cheap, environmentally friendly, and sustainable development. Up to now, various porous biochars have been reported as S hosts for Li-S batteries[26,27]. As a natural biomass, cotton has been widely used in daily life due to its excellent sustainability.

In this work, we proposed a simple yet effective strategy to turn biomass cotton into heteroatom-doped porous biochar fibers with a hierarchical pore structure. Typically, N, S dual-doped porous biochar fibers (PBF@N@S) were prepared through a simple one-step potassium hydroxide (KOH) activation method. The as-prepared carbons have a unique interconnected porous structure with N, S co-doping, which is beneficial to the impregnation of S. The as-fabricated S/PBF@N@S composite electrode exhibited an excellent specific capacity with high cycling performance.

EXPERIMENTAL

Materials and apparatus

Cystine, KOH, melamine, and nmethyl-2-pyrrolidene (NMP) solution was supplied by Sinopharm Chemical Reagent Co., Ltd. (China). X-ray diffraction (XRD) patterns were tested on a Rigaku Smartlab (9) diffractometer with Cu Kα radiation. The testing range of two-theta was from 5° to 90°, and the scanning rate of 10°/min with a step of 0.02°. Scanning electronic microscopy (SEM) images were obtained with a Hitachi SU8020 electron microscopy. Transmission electron microscopy (TEM) measurements were performed with a JEOL JEM-2100F field emission transmission electron microscope. Raman spectra were obtained using a Renishaw INVIA Raman spectrometer. Gas adsorption/desorption isotherms were obtained from a Quadrasorb SIMP analyzer at the liquid nitrogen temperature. The specific surface area of the carbons was calculated using the Brunauer-Emmett-Teller (BET) equation. X-ray photoelectron spectroscopy (XPS) measurements were conducted on Thermo Fisher Scientific ESCALAB 250Xi equipment. All spectra were calibrated with the binding energy of the C1s peak at 284.8 eV.

Preparation of PBF@N@S

The preparation of PBF@N@S is shown in Figure 1. Firstly, the cotton was cleaned and cut into cotton patches using scissors and ground into fine fibers. Cystine was used as N and S sources, and the fine cotton fibers were mixed with KOH/cystine at 60 ℃ for three days with the weight ratio of 1:5. After drying in an oven, pyrolysis was conducted by heating under flowing argon at 800 ℃ with a heating rate of 10 ℃/min with a hold period of 1 h at 800 ℃. For comparison, N-doped porous biochar fibers (PBF@N) were obtained as the same process but using melamine as a N source. In addition, bare biochar fibers (PBF) were obtained by directly carbonizing fine cotton fibers without the use of KOH, cystine, and melamine. Subsequently, all the carbonized products were cleaned using deionized water and anhydrous ethanol.

Electrode preparation and electrochemical measurements

The cathode slurry was prepared by mixing as-prepared carbons (PBF, PBF@N, or PBF@N@S), S with polyvinylidene fluoride (PVDF), and carbon black at a mass ratio of 8:1:1 in NMP solution. The mixed slurry was then coated on an aluminum foil and vacuum dried at 60 ℃ overnight. The S loading is the same mass ratio as carbons (1:1 mass ratio of S to carbon, named PBF-S-50%, PBF@N-S-50%, and PBF@N@S-S-50%). Coin cells (2032 type) were assembled using lithium foil as the anode and Celgard 3501 sheets as the separator. 35 μL of 1 M lithium bis (trifluoromethanesulfonyl)imide (LiTFSI) in a mixed solvent of 1,2-dimethoxyethane (DME) and 1,3-dioxolane (DOL) with a volumetric ratio of 1:1 with 1 wt% of $LiNO_3$ were used as electrolyte. Electrochemical properties were performed on MTI BST8-MA (MTI Corporation) and Arbin BT2143 battery analyzers. The applied voltage window was from 1.8 to 2.8 V. All batteries were assembled in a glovebox.

RESULTS AND DISCUSSION

Characterization of PBFs

Figure 2A shows the XRD patterns of the as-prepared porous carbon samples. All samples show two broad peaks, located at around 25° and 43° two-theta, which are assigned to the reflection of the graphite (002) and (101) planes (JCPDS Card File, No. 41-1487), respectively[23]. No other observable peaks due to impurities have appeared. In addition, as it can be seen, the graphite peak of PBF@N@S is sharper, particularly than the others, which proves that PBF@N@S has better crystallization. Raman spectra are exhibited in Figure 2B, two characteristic peaks at around 1,350 and 1,600 cm^{-1} can be observed, corresponding to the *D* and *G* bands of carbon, respectively[28]. The ratio of the *D* band to the *G* band (I_D/I_G) is usually used to evaluate the density of defective sites[23]. The I_D/I_G ratio is 1.11 for PBF@N@S, 1.01 for PBF@N, and 0.98 for PBF, respectively, indicating that the defect density increased. The improved defect density would lead to more electrochemical active sites[23].
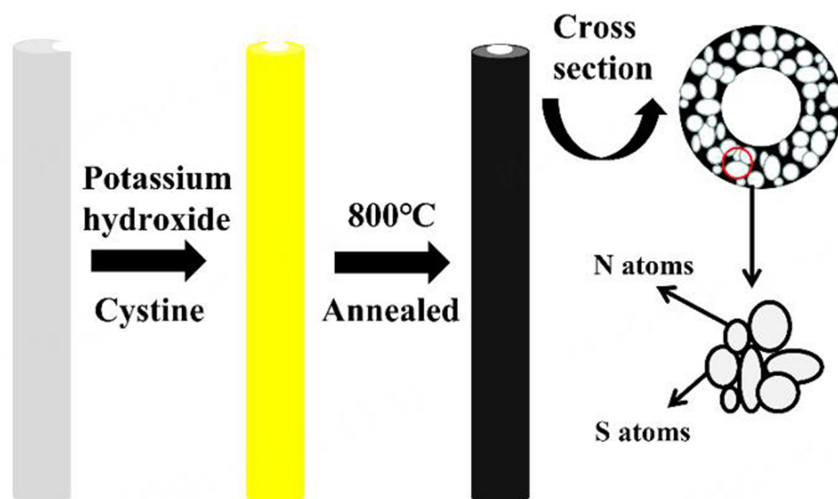
Figure 1. A schematic diagram of preparing PBF@N@S. PBF@N@S: N, S dual-doped porous biochar fibers.
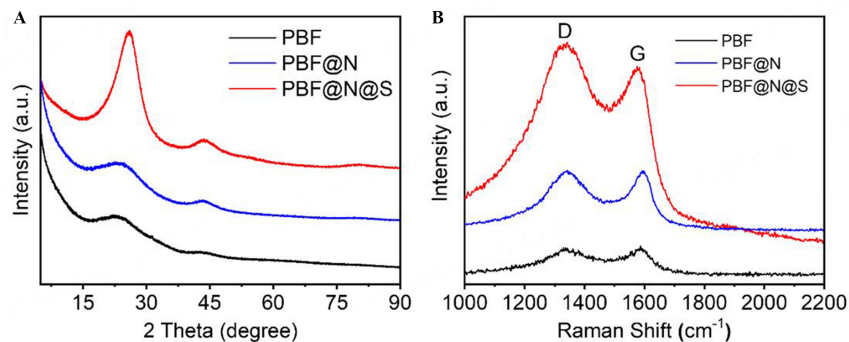
Figure 2. (A) XRD patterns of the PBF, PBF@N, and PBF@N@S and (B) Raman spectra of PBF, PBF@N, and PBF@N@S. PBF@N: N-doped porous biochar fibers; PBF@N@S: N, S dual-doped porous biochar fibers; XRD: X-ray diffraction.
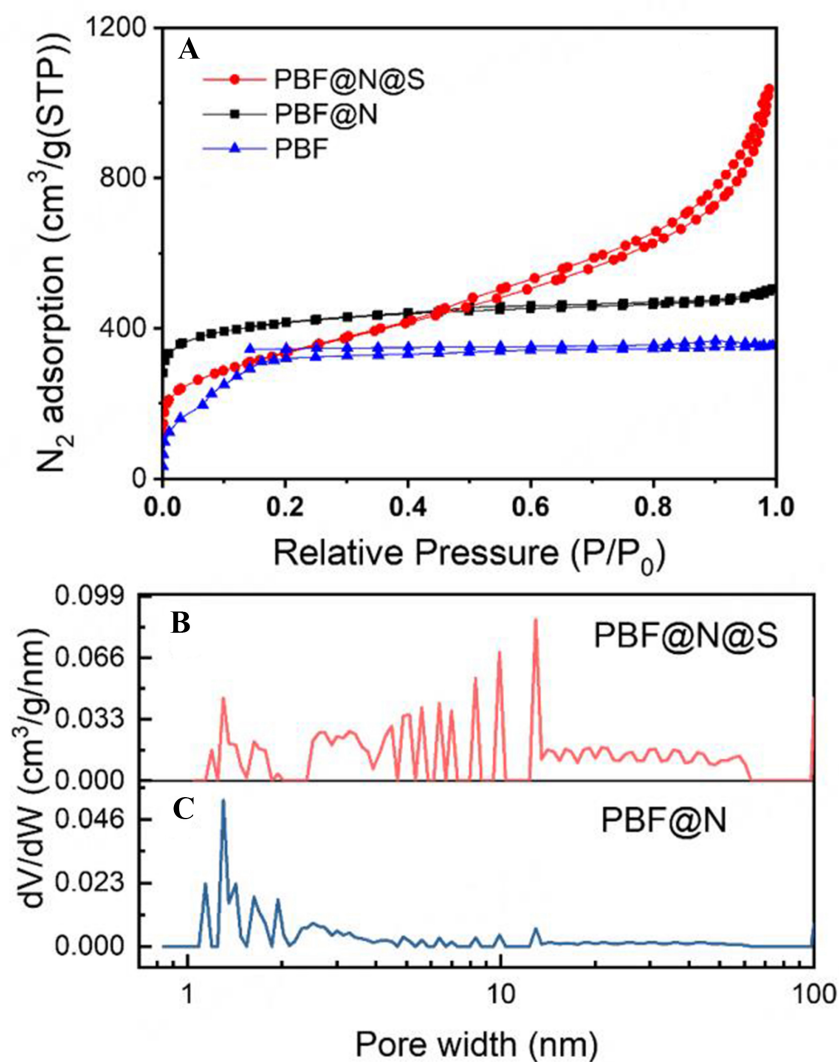
N adsorption/desorption isotherms are used to characterize the porosity of the samples, as illustrated in Figure 3A, and the corresponding pore size distribution is shown in Figure 3B-C. As shown in Figure 3A, the PBF@N@S shows a combination of *Type I* and *II* isotherms with an obvious H4 hysteresis loop, indicating that both micropores and mesopores exist. PBF@N also shows a composite of *type I* and *II* isotherms but with a small hysteresis loop, indicating a micropore dominant characteristic. PBF shows poor gas adsorption-desorption properties. The calculated BET surface area is 1,696 m^2/g, 1,342 m^2/g, and 35 m^2/g for PBF@N@S, PBF@N, and PBF, respectively, as presented in Table 1. A greater specific surface area would lead to better contact between the material and the electrolyte and further improve the capacity and cycle stability[29]. Moreover, the corresponding pore size distribution of the two porous materials is exhibited in Figure 3B-C. It can be seen from Figure 3B that multiple pore systems of different sizes in PBF@N@S are found, whereas the pore sizes in PBF@N are mostly distributed below 2 nm. The hierarchical pore structure of PBF@N@S is not only beneficial for the inclusion of more S but also can bind polysulfide.

The morphologies of PBF, PBF@N, and PBF@N@S were studied by SEM and TEM. As can be seen from Figure 4A, the PBF remains the structure of fibers, which shows a smooth surface and no porous structure. PBF@N (Figure 4B) and PBF@N@S (Figure 4C-D) exhibit large amounts of pore structures, which originates from the activation of KOH. According to Figure 4C-D, the large pores connect with each other

**Table 1. Physical characteristics of PBF, PBF@N, and PBF@N@S**

Sample	BET surface area (m^2/g)
PBF	35
PBF@N	1342
PBF@N@S	1696

BET: Brunauer-Emmett-Teller; PBF: Bare biochar fibers; PBF@N: N-doped porous biochar fibers; PBF@N@S: N, S dual-doped porous biochar fibers.

Figure 3. N_2 adsorption/desorption isotherms of PBF, PBF@N, and PBF@N@S (A) and pore size distribution of the PBF@N@S (B) and PBF@N (C). PBF: Bare biochar fibers; PBF@N: N-doped porous biochar fibers; PBF@N@S: N, S dual-doped porous biochar fibers.

with a pore size of 1-2 μm in the PBF@N@S. In addition, it can be seen from Figure 4D that plenty of small-scale pores exist and interconnect. The three-dimensional macro-porous structure of the carbon materials played a vital role in enabling high S loading, physically limiting the polysulfide, and improving the capacity and cycling stability[30,31].
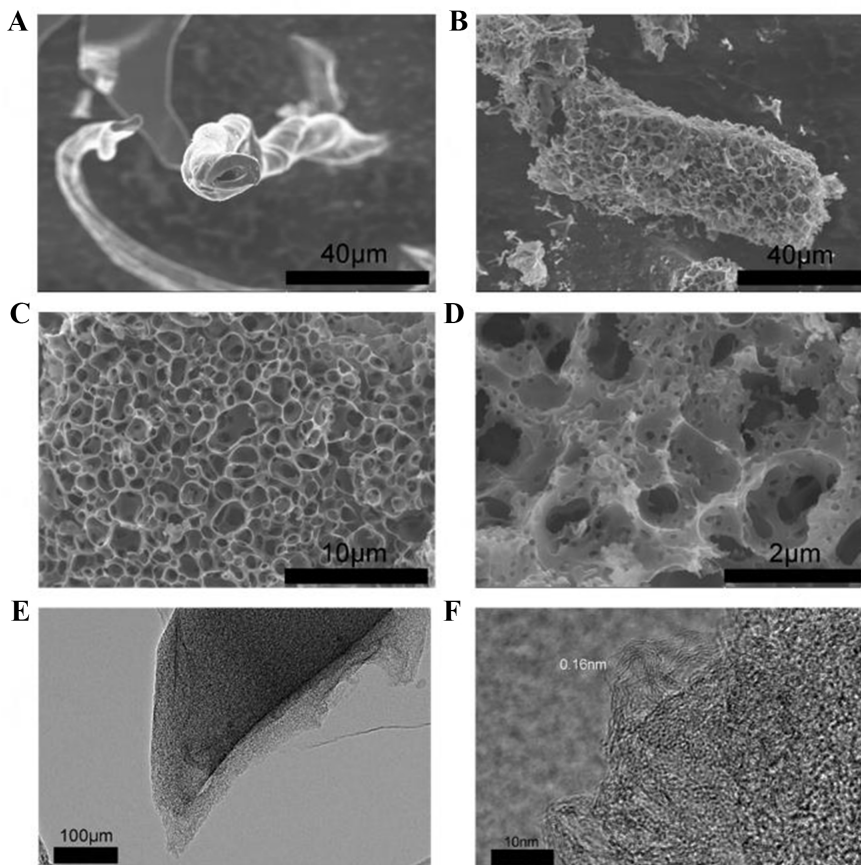
Figure 4. SEM images of PBF (A), PBF@N (B), and PBF@N@S (C-D) and TEM images of the PBF@N@S (E-F). PBF: Bare biochar fibers; PBF@N: N-doped porous biochar fibers; PBF@N@S: N, S dual-doped porous biochar fibers; SEM: scanning electronic microscopy; TEM: transmission electron microscopy.

TEM also exhibits the formation of an abundant porous structure in the sample PBF@N@S. As shown in Figure 4E and Figure 4F, the abundant microporous structure has small pore sizes, of which most of them are smaller than 2 nm. The abundant microporous structure is beneficial to restrict the volume change of the S due to the strong confinement effect and contributes to the physical adsorption slowing down the S loss. Meanwhile, the crystal lattice of PBF@N@S is hardly observed from the high-resolution TEM image [Figure 4F], indicating an irregular carbon, which has a positive effect on bundling polysulfide.

XPS is used to study the chemical characteristics of the surface of the PBF@N@S. Figure 5A shows the wide-scan survey XPS spectrum of the PBF@N@S. The obvious signals of C, N, and S further reveal the N and S co-doping. The C 1s high-resolution spectrum [Figure 5B] could be deconvoluted into five peaks at 284.8 eV, 286.1 eV, 287.2 eV, 288.4 eV, and 289.7 eV, relating to C-C/C=C, C-N/C-S, C-O, C=O, and O-C=O bonds, respectively[29,32-34]. Figure 5C shows N 1s spectra, which can be effectively divided into pyridinic N (398.4 eV), pyrrolic N (400.3 eV), and quaternary N (401.8 eV)[23]. The S 2p spectra are shown in Figure 5D. The two sulfur species are assigned to carbon-bonded thiophene-like sulfur C-S-C[29,35]. The co-doped N and S would improve the polysulfide absorptivity and long-term cycling stability[29]. In addition, the atomic percentages of PBF@N@S obtained from XPS are listed in Table 2, which shows the N and S atomic contents are 3.18% and 1.34%, respectively.

Table 2. Elemental composition of PBF@N@S obtained from XPS

Elements	C	N	S	O
Percentage (at.%)	81.44	3.18	1.34	14.04

PBF@N@S: N, S dual-doped porous biochar fibers; XPS: X-ray photoelectron spectroscopy.
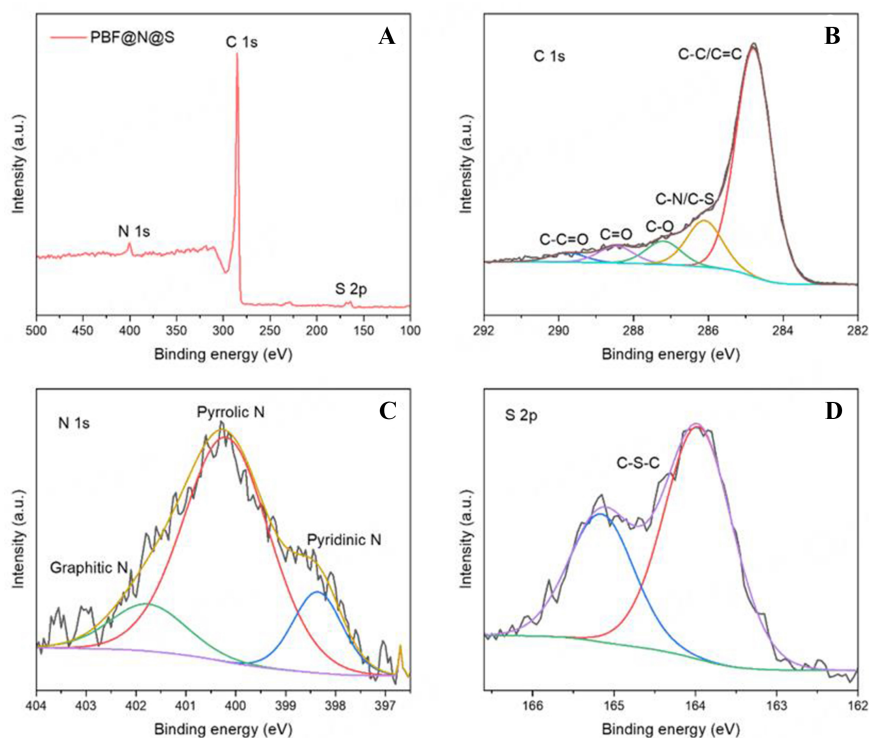
Figure 5. XPS spectra of PBF@N@S: full survey (A), C 1s spectra (B), N 1s spectra (C), and S 2p spectra (D). PBF@N@S: N, S dual-doped porous biochar fibers; XPS: X-ray photoelectron spectroscopy.

Electrochemical measurements

To investigate the electrochemical properties of the cathode, electrochemical cycling was first implemented. Figure 6A illustrates the cycling performances of PBF-S-50%, PBF@N-S-50%, and PBF@N@S-S-50% at a current rate of 0.1C. All these three electrodes showed high discharge capacities even after 200 cycles. Obviously, it demonstrates the cycling performance of PBF@N@S-S-50% electrodes is much better than PBF@N-S-50% and PBF-S-50%. The introduction of N and S atoms into the PBF induces asymmetric sites for binding lithium polysulfide, which enables the PBF@N@S electrode to have higher capacity and battery cycling stability. On the other hand, the hierarchical porous structure of PBF@N@S ensures good electrical contact between S and the conductive carbon framework and further accelerates Li-ions transportation, which improves the high performance of the battery.

Furthermore, an excellent rate capability performance is observed in Figure 6B. With the C rate successively increasing from 0.1 to 0.2, 0.5, 1, and 2C, the capacity of the three electrodes gradually decreases. When the C rate switches back to 0.1C after 50 cycles, the capacity of the electrodes can be recovered to the initial stage, indicative of their good rate capability. Notably, it is evident that PBF@N@S-S-50% exhibits consistently better electrochemical performance than both PBF@N-S-50% and PBF-S-50% cathodes, including larger specific capacity, longer cyclic life, and superior rate capability.
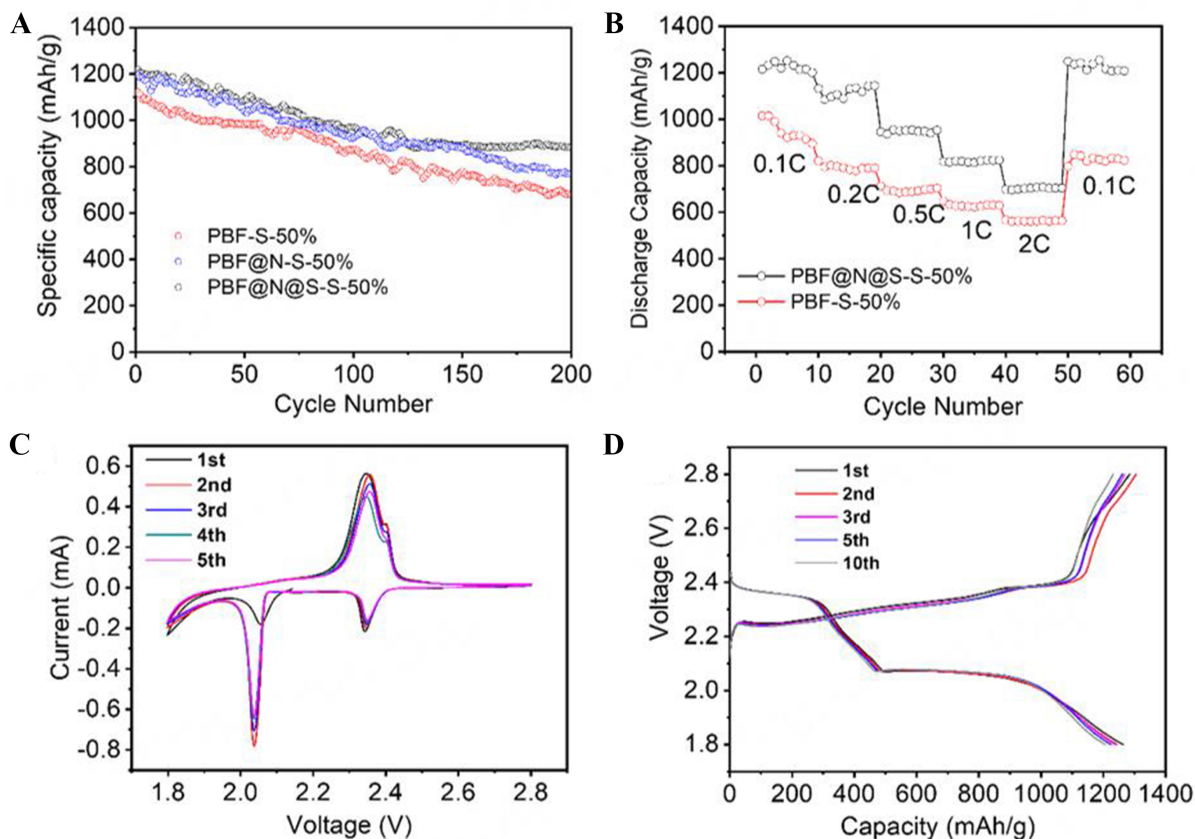
Figure 6. Electrochemical performances of as-prepared electrode for Li-S batteries: (A) Cycling performance of the PBF-S-50%, PBF@N-S-50%, and PBF@N@S-S-50% electrode over 200 cycles at 0.1C; (B) Rate capability of PBF@N@S-S-50%, PBF@N-S-50%, and PBF-S-50%; (C) CV profiles of PBF@N@S-S-50% electrode at the scan rate of 0.1 mV/s; (D) Galvanostatic charge-discharge curves of the PBF@N@S-S-50% at 0.1C. PBF: Bare biochar fibers; PBF@N: N-doped porous biochar fibers; PBF@N@S: N, S dual-doped porous biochar fibers.

The electrochemical mechanism of a Li-S battery was studied by cyclic voltammetry (CV), as shown in Figure 6C. The typical CV curves of a S cathode contain two reductive peaks and one oxidative peak. During the cathodic scan, peaks at around 2.35 V were attributed to the transformation from solid sulfur to soluble polysulfide intermediates (S_n^{2-}, n ⩾ 4)[36,37]. The other reduction peak that appeared at around 2.02 V can be agreed with the reaction of polysulfide to the lower order insoluble Li_2S_2 and finally to Li_2S from small sulfur molecule S_4^{2-}[38,39]. Subsequently, the anodic peak at around 2.35 V was coherent with the conversion of Li_2S_2/Li_2S to polysulfides and sulfur. Meanwhile, the peak position and area remained nearly good reaction reversibility in the successive cycles, indicating good stability.

Typical voltage capacity profiles of the PBF@N@S-S-50% at different cycles are shown in Figure 6D. The discharge curves show two typical plateaus, which locate at around 2.1 V and 2.3 V, respectively; this could be assigned to a two-step reaction of S with Li during the discharge process, agreeing well with the results of CV measurements. In addition, the plateau at about 2.1 V could be commonly observed, which might originate from the strong adsorption process of Li_2S_2 on the microporous besides the reduction process (from Li_2S_2 to Li_2S). This observation is similar to other carbon-sulfur nanocomposite electrodes[40,41]. Such strong interactions can guarantee the stable performance of PBF@N@S-S-50% electrodes. Moreover, the discharge plateaus are considerably stable even after ten cycles, which ensures excellent cyclic performance.
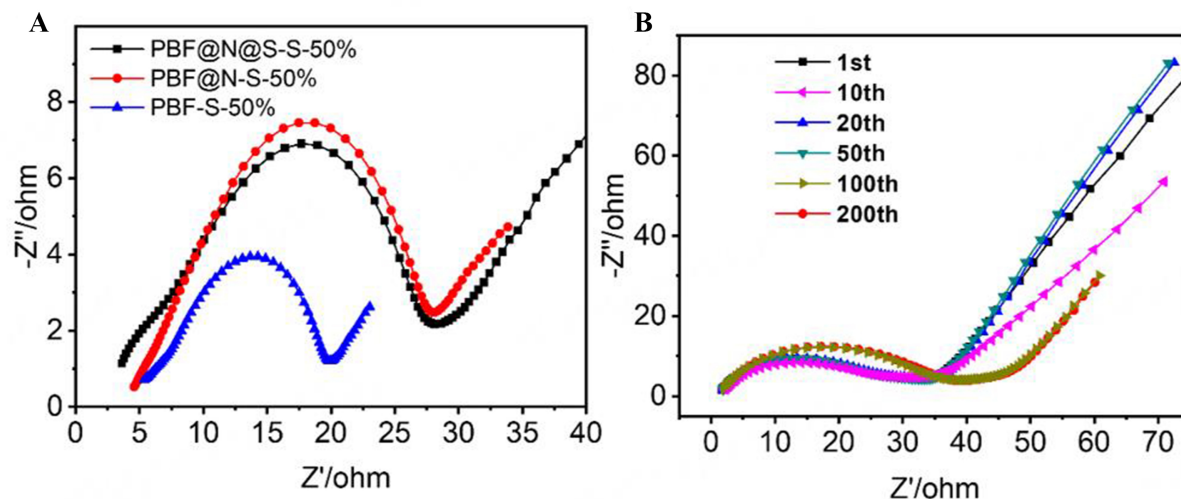
Figure 7. Nyquist plots of PBF@N@S-S-50%, PBF@N-S-50%, and PBF-S-50% cathodes (A) and Nyquist plots of PBF@N@S-S-50% after 1st, 10th, 20th, 50th, 100th, and 200th cycles (B). PBF: Bare biochar fibers; PBF@N: N-doped porous biochar fibers; PBF@N@S: N, S dual-doped porous biochar fibers.

Electrochemical impedance spectroscopy (EIS) is a powerful method for analyzing cyclic changes and was measured to get further insight into the electrochemical performance. The semicircle at medium-to-high frequency was attributed to the charge-transfer process at the interface between the electrolyte and electrode[42]. The Warburg impedance that occurred in low frequency was associated with the semi-infinite diffusion of soluble lithium polysulfide in the electrolyte[43,44]. Figure 7A shows the Nyquist plots of fresh PBF@N@S-S-50%, PBF@N-S-50%, and PBF-S-50% cathodes. The introduction of N and S atoms makes the impedance of PBF@N@S and PBF@N much larger than PBF. Figure 7B exhibits the EIS plots of PBF@N@S-S-50% after the 1st, 10th, 20th, 50th, 100th, and 200th cycles. As shown in Figure 7, after activation of the first cycle, the resistance gradually became quite stable and maintained a small charge-transfer resistance even at 200 cycles. As the number of charge-discharge cycles increased, the impedance of the PBF@N@S-S-50% increased gradually and then became stable because of the solid-electrolyte-interface (SEI) film, which was caused by the formation of Li_2S (or Li_2S_2) on the carbon matrix in the cathode[45]. This small and stable resistance should also benefit the cycling performance.

CONCLUSIONS

A N, S co-doped hierarchical porous carbon has been successfully prepared *via* a simple one-step activation method and was employed as a cathode in Li-S batteries. The obtained porous carbon shows a highly interconnected network, which can encapsulate sulfur and polysulfide. The co-doped N and S into the carbon matrix could generate more active sites, which improves the battery capacity and cycling stability. The electrode illustrated an improved electrochemical performance and delivered a high initial capacity (above 1,200 mAh/g at 0.1C) and high reversible capacity after 200 cycles. This work provides a facile route to synthesize heteroatom-doped porous carbon materials for Li-S battery applications.

DECLARATIONS

Authors' contributions

Conceptualization, methodology, investigation, writing, review & editing: Li X
Conceptualization, writing, review & editing: Sun K

Availability of data and materials
Not applicable.

Financial support and sponsorship
None.

Conflicts of interest
All authors declared that there are no conflicts of interest.

Ethical approval and consent to participate
Not applicable.

Consent for publication
Not applicable.

REFERENCES

1. Qin J, Yang Z, Xing F, Zhang L, Zhang H, Wu Z. Two-dimensional mesoporous materials for energy storage and conversion: current status, chemical synthesis and challenging perspectives. *Electrochem Energy Rev* 2023;6:9. DOI
2. Li F, Liu R, Liu J, Li H. Voltage hysteresis in transition metal oxide cathodes for Li/Na-Ion batteries. *Adv Funct Materials* 2023;33:2300602. DOI
3. Wu X, He G, Ding Y. Dealloyed nanoporous materials for rechargeable lithium batteries. *Electrochem Energ Rev* 2020;3:541-80. DOI
4. Li M, Lu J, Chen Z, Amine K. 30 years of lithium-ion batteries. *Adv Mater* 2018;30:e1800561. DOI
5. Li H, Zhang W, Sun K, et al. Manganese-based materials for rechargeable batteries beyond lithium-ion. *Adv Energy Mater* 2021;11:2100867. DOI
6. Xin S, Chang Z, Zhang X, Guo Y. Progress of rechargeable lithium metal batteries based on conversion reactions. *Natl Sci Rev* 2017;4:54-70. DOI
7. Kim J, Lee D, Jung H, Sun Y, Hassoun J, Scrosati B. An advanced lithium-sulfur battery. *Adv Funct Mater* 2013;23:1076-80. DOI
8. Li L, Wu ZP, Sun H, et al. A foldable lithium-sulfur battery. *ACS Nano* 2015;9:11342-50. DOI PubMed
9. Tao T, Lu S, Fan Y, Lei W, Huang S, Chen Y. Anode improvement in rechargeable lithium-sulfur batteries. *Adv Mater* 2017;29:1700542. DOI PubMed
10. Liu B, Fang R, Xie D, et al. Revisiting scientific issues for industrial applications of lithium-sulfur batteries. *Energy Environ Mater* 2018;1:196-208. DOI
11. Zhao X, Cheruvally G, Kim C, et al. Lithium/sulfur secondary batteries: a review. *J Electrochem Sci Technol* 2016;7:97-114. DOI
12. Wang M, Bai Z, Yang T, et al. Advances in high sulfur loading cathodes for practical lithium-sulfur batteries. *Adv Energy Mater* 2022;12:2201585. DOI
13. Manthiram A, Fu Y, Su YS. Challenges and prospects of lithium-sulfur batteries. *Acc Chem Res* 2013;46:1125-34. DOI PubMed
14. Huang L, Li J, Liu B, et al. Electrode design for lithium-sulfur batteries: problems and solutions. *Adv Funct Mater* 2020;30:1910375. DOI
15. Zhang Q, Cheng X, Huang J, Peng H, Wei F. Review of carbon materials for advanced lithium-sulfur batteries. *Carbon* 2015;81:850. DOI
16. Xu Z, Kim J, Kang K. Carbon nanomaterials for advanced lithium sulfur batteries. *Nano Today* 2018;19:84-107. DOI
17. Liu H, Jia G, Zhu S, Sheng J, Zhang Z, Li Y. Functionalized carbon-based composite materials for cathode application of lithium-sulfur batteries. *Acta Chimica Sinica* 2022;80:89-97. DOI
18. Zhang SS. Heteroatom-doped carbons: synthesis, chemistry and application in lithium/sulphur batteries. *Inorg Chem Front* 2015;2:1059-69. DOI
19. Yang J, Xie J, Zhou X, et al. Functionalized N-Doped porous carbon nanofiber webs for a lithium-sulfur battery with high capacity and rate performance. *J Phys Chem C* 2014;118:1800-7. DOI
20. Niu S, Lv W, Zhou G, et al. N and S co-doped porous carbon spheres prepared using L-cysteine as a dual functional agent for high-

performance lithium-sulfur batteries. *Chem Commun* 2015;51:17720-3. DOI

21.   Kim E, Lee AS, Lee T, et al. Organic dye-derived N, S co-doped porous carbon hosts for effective lithium polysulfide confinement in lithium-sulfur batteries. *Nanomaterials* 2021;11:2954. DOI PubMed PMC

22.   Díez N, Sevilla M, Fuertes AB. N/S-co-doped porous carbon nanoparticles serving the dual function of sulfur host and separator coating in lithium-sulfur batteries. *ACS Appl Energy Mater* 2020;3:3397-407. DOI

23.   Sun K, Wang C, Tebyetekerwa M, Zhao XS. Electrocapacitive desalination with nitrogen-doped hierarchically structured carbon prepared using a sustainable salt-template method. *Chem Eng J* 2022;446:137211. DOI

24.   Kim DK, Seul Byun J, Moon S, Choi J, Ha Chang J, Suk J. Molten salts approach of metal-organic framework-derived nitrogen-doped porous carbon as sulfur host for lithium-sulfur batteries. *Chem Eng J* 2022;441:135945. DOI

25.   Yang H, Yang Y, Zhang X, et al. Nitrogen-doped porous carbon networks with ACtive Fe-Nx sites to enhance catalytic conversion of polysulfides in lithium-sulfur batteries. *ACS Appl Mater Interfaces* 2019;11:31860-8. DOI PubMed

26.   Benítez A, Amaro-gahete J, Chien Y, Caballero Á, Morales J, Brandell D. Recent advances in lithium-sulfur batteries using biomass-derived carbons as sulfur host. *Renew Sust Energ Rev* 2022;154:111783. DOI

27.   Liu P, Wang Y, Liu J. Biomass-derived porous carbon materials for advanced lithium sulfur batteries. *J Energy Chem* 2019;34:171-85. DOI

28.   Li G, Sun J, Hou W, Jiang S, Huang Y, Geng J. Three-dimensional porous carbon composites containing high sulfur nanoparticle content for high-performance lithium-sulfur batteries. *Nat Commun* 2016;7:10601. DOI PubMed PMC

29.   Pang Q, Tang J, Huang H, et al. A nitrogen and sulfur dual-doped carbon derived from polyrhodanine@cellulose for advanced lithium-sulfur batteries. *Adv Mater* 2015;27:6021-8. DOI

30.   Yu X, Yin Y, Ma C, et al. N-doped porous carbon@CNT nanowire as effective polysulfides adsorption-catalysis interlayer for high-performance lithium-sulfur batteries. *Chem Eng Sci* 2023;268:118400. DOI

31.   Tomer VK, Malik R, Tjong J, Sain M. State and future implementation perspectives of porous carbon-based hybridized matrices for lithium sulfur battery. *Coord Chem Rev* 2023;481:215055. DOI

32.   Peng W, Han G, Huang Y, Cao Y, Song S. Insight the effect of crystallinity of natural graphite on the electrochemical performance of reduced graphene oxide. *Results Phys* 2018;11:131-7. DOI

33.   Schroer ZS, Wu Y, Xing Y, et al. Nitrogen-sulfur-doped graphene quantum dots with metal ion-resistance for bioimaging. *ACS Appl Nano Mater* 2019;2:6858-65. DOI

34.   Yang Z, Dai Y, Wang S, Cheng H, Yu J. In situ incorporation of a S, N doped carbon/sulfur composite for lithium sulfur batteries. *RSC Adv* 2015;5:78017-25. DOI

35.   Chen M, Zhao S, Jiang S, et al. Suppressing the polysulfide shuttle effect by heteroatom-doping for high-performance lithium-sulfur batteries. *ACS Sustainable Chem Eng* 2018;6:7545-57. DOI

36.   Bao W, Su D, Zhang W, Guo X, Wang G. 3D metal carbide@mesoporous carbon hybrid architecture as a new polysulfide reservoir for lithium-sulfur batteries. *Adv Funct Mater* 2016;26:8746-56. DOI

37.   Wang D, Liu J, Bao X, Qing C, Zhu T, Wang H. Macro/mesoporous Carbon/defective TiO_2 composite as a functional host for lithium-sulfur batteries. *ACS Appl Energy Mater* 2022;5:2573-9. DOI

38.   Lei D, Li J, Xiang M, et al. Synergistic constraint and conversion of lithium polysulfide using a 3D hollow carbon interlayer in ultrahigh sulfur content Li-S batteries. *Appl Surf Sci* 2023;623:157080. DOI

39.   Zhang H, An Y, Li S, et al. Honeycomb porous N-doped carbon synergized with ultrafine Ni_2P electrocatalyst for boosting polysulfide conversion in lithium-sulfur batteries. *Electrochimica Acta* 2023;445:142047. DOI

40.   Wen Y, Wang X, Huang J, Li Y, Li T, Ren B. Coffee grounds derived sulfur and nitrogen dual-doped porous carbon for the cathode material of lithium-sulfur batteries. *Carbon Lett* 2023;33:1265-78. DOI

41.   Li M, Liu Z, Tan L, et al. Fabrication of cubic and porous carbon cages with in-situ-grown carbon nanotube networks and cobalt phosphide for high-capacity and stable lithium-sulfur batteries. *ACS Sustainable Chem Eng* 2022;10:10223-33. DOI

42.   Ma L, Liu Q, Zhu H, Liu L, Kang C, Ji Z. Flower-like $Ni_3Sn_2@Ni_3S_2$ with core-shell nanostructure as electrode material for supercapacitors with high rate and capacitance. *J Colloid Interface Sci* 2022;626:951-62. DOI

43.   Peng W, Wang W, Han G, Huang Y, Zhang Y. Fabrication of 3D flower-like MoS_2/graphene composite as high-performance electrode for capacitive deionization. *Desalination* 2020;473:114191. DOI

44.   Sun M, Wang X, Li Y, Zhao Z, Qiu J. Integration of desulfurization and lithium-sulfur batteries enabled by amino☐functionalized porous carbon nanofibers. *Energy & Environ Materials* 2023;6:e12349. DOI

45.   Liang Z, Shen J, Xu X, et al. Advances in the development of single-atom catalysts for high-energy-density lithium-sulfur batteries. *Adv Mater* 2022;34:e2200102. DOI